Planar Trigger Switch and Its Integrated Chip With Exploding Foil Initiator Based on Low-Temperature Cofired Ceramic

Qiu Zhang, Cong Xu, Peng Zhu, Guili Yang, Zhi Yang, and Ruiqi Shen

***Abstract*—A planar trigger switch constituting of three electrodes was designed and fabricated using low-temperature cofired ceramic, and characterized under an atmospheric pressure. The results showed that when the operating voltage ranges between 77.2% and 86.8% of its self-breakdown voltage, the inductance of the switch was lower than that of commercial spark gap switch by approximately 60 nH, the current rising time was shortened by nearly 1/2, and the peak current increased by about 30%. The peak current and rising edge were 4000 A and 146 ns at 0.22 μF/2.0 kV, respectively, which was in agreement with simulation values well. Subsequently, the switch was devised to be *in situ* integrated with an exploding foil initiator together. The electrical characterizations were performed on the chip, obtaining the switch's rapid turn-ON time of 29 ns and a large current density of 1.08×10^8 A·cm^{-2} at 0.22 μF/2.25 kV. Furthermore, photon Doppler velocimetry was exploited to capture the detailed trajectory of a 50-μm-thick flyer with an extracted terminal velocity of 2200 m/s. Finally, boron–potassium nitrate pellets and hexanitrostilbene pellets were used to successfully verify the practicability of the chip in the ignition and detonation of explosives.**

***Index Terms*—Electroexplosive devices, integrated circuits, spark gaps switch.**

I. Introduction

EXPLODING foil initiator (EFI), also known as slapper detonator, has been widely used in ignition and detonation sequences [1]–[3]. One advantage of an EFI is that the exploding metal foil and explosive charge are physically separated by a thin insulating material and an air gap. This contributes to safety since it eliminated the spurious current that might cause accidental firing [4]–[7]. Generally, the EFI is placed in a capacitor discharge circuit. It consists of three real, physical components: a capacitor, a discharge switch, and the load (i.e., EFI). Among them, the switch is the most important part which must work at high speed and allow the energy stored in a capacitor to be couple into an EFI quickly. Several kinds of switches are designed and fabricated for pulse power applications, such as three-elements gas or vacuum switch, metal oxide semiconductor-controlled thyristor, scalable power semiconductor switch, power MOSFET devices and insulated gate bipolar transistor [8]–[12]. Of these, the three-electrode spark gap switch is the most commonly used for its low leakage, radiation hardness, and robustness [13]. However, this type switch has a cylindrical structure and huge configuration, which means that it is hard to be connected with strip transmission line. Besides that, the complicated production process and piece-part assembly will also result in imprecision and high cost.

With the increasing miniaturization requirements on the electric ignition/initiation device, an EFI inserted with a planar switch to achieve a compact monolithic structure becomes a promising uptrend for the development of EFI. Currently, the main technical difficulties for the miniaturized devices rest with the design of a low-inductance discharge circuit and the development of a short-time response switch that allows a large current to flow through [14]–[16]. The smaller the inductance in the loop is, the quicker the conduction of the switch is. Thus, the more energy can be deposited into the exploding foil.

Baginski proposed a micromachined planar triggered spark gap switch capable of operating at high speeds and over a wide range of voltages and energies [17]. However, there is no report on the integration of a spark gap switch and an EFI until this study.

In this study, we devised a planar trigger switch with low-temperature cofired ceramic (LTCC) techniques, and the switch was designed to be *in situ* incorporated with an EFI, thus forming a Switch-EFI integrated chip (or "S-EFI chip" for short). Since the substantial advantages of LTCC are batch production and one-step preparation without any precise positioning or a bonding process [18], [19], so as to ensure that the planar triggered switch and the integrated chip are low cost and consistent in performance, benefiting those experiments that require accurate time control and a large number of destructive testing.

II. Design, Fabrication, and Characterization of the Planar Trigger Switch

A. Design and Fabrication

With reference to the conventional spark gap switch configuration, we designed three electrodes for the planar trigger switch,

Manuscript received March 28, 2019; revised April 30, 2019; accepted June 16, 2019. Date of publication June 23, 2019; date of current version December 13, 2019. This paper is not prepared for a conference or others, and this is the first time the paper has been submitted to an academic journal. This work was supported by the Natural Science Foundation of Jiangsu Province under Grant BK20151486. Recommended for publication by Associate Editor K. Ngo. *(Corresponding author: Peng Zhu.)*

Q. Zhang, C. Xu, P. Zhu, Z. Yang, and R. Shen are with the School of Chemical Engineering, Nanjing University of Science and Technology, Nanjing 210094, China (e-mail: qiuzhang@njust.edu.cn; congxu@njust.edu.cn; zhupeng@njust.edu.cn; yangzhi@njust.edu.cn; rqshen@njust.edu.cn).

G. Yang is with the Field Engineering College, Army Engineering of PLA, Nanjing 210007, China (e-mail: 50509100@qq.com).

Color versions of one or more of the figures in this paper are available online at http://ieeexplore.ieee.org.

Digital Object Identifier 10.1109/TPEL.2019.2924801

See http://www.ieee.org/publications_standards/publications/rights/index.html for more information.

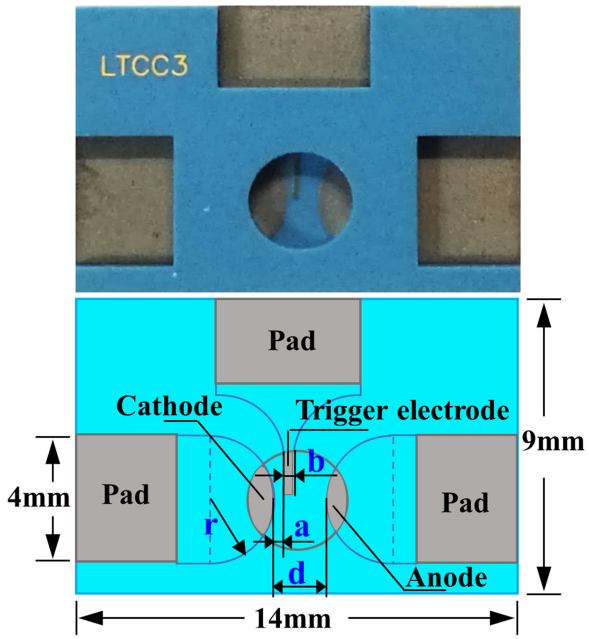

Fig. 1. Photograph and the diagram of planar trigger switch by LTCC.

where one of the three electrodes was a ground or common connection, one of the other electrodes was the trigger electrode and the third was the high-voltage input. The photograph and the diagram of the planar triggered switch were shown in Fig. 1. Generally, the breakdown voltage of an air gap in a quasi-uniform electric field obeyed the following empirical formula [20]:

$$U_b = \frac{(2.44pd + 2.12\sqrt{pd})}{\delta} \tag{1}$$

where U_b was the self-breakdown voltage in kilovolts, p was the air pressure in bars, d was the gap distance in millimeters, and δ was the field enhancement factor, which was defined as the ratio between the maximum and the mean field strength in the gap. For the planar semicircular electrodes designed in this paper, δ could be approximately estimated as follows [21]:

$$\delta \approx \frac{P + \sqrt{P^2 + 8}}{4} \tag{2}$$

where $P = 1 + d/r$, which was a constant, r was the actual electrode radius, and herein $r = 1$ mm. Assuming $d = 0.9$ mm, then δ was 1.33. Considering the shrinkage caused by sintering process of ceramics, δ was taken as 1.4. In order to make the switch withstand no less than 2.7 kV at standard atmospheric pressure, the electrode space d could be calculated with formula (1) to be 0.78 mm. For a certain margin, the gap distance d was taken as 0.9 mm. Additionally, we set the trigger electrode in an offset position "a" relative to the center of the left cathode, which was 150 μm. This design was intended to minimize the triggered arc length, thereby ensuring the lifetime of the trigger electrode while satisfying the breakdown requirements. Similarly, we set the trigger electrode width "b" to be 200 μm, which was the minimum line width achieved by processing, in order to obtain a wide range of operating voltages.

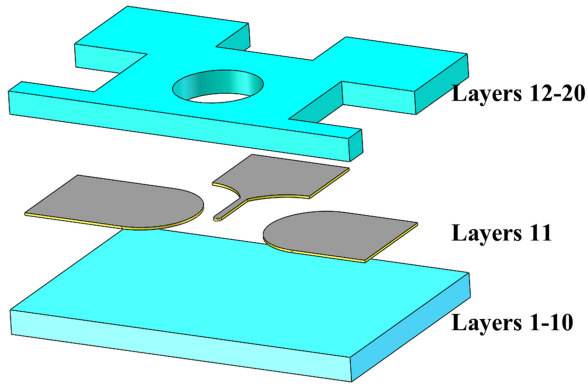

Fig. 2. Exploded view of the fabrication of switch.

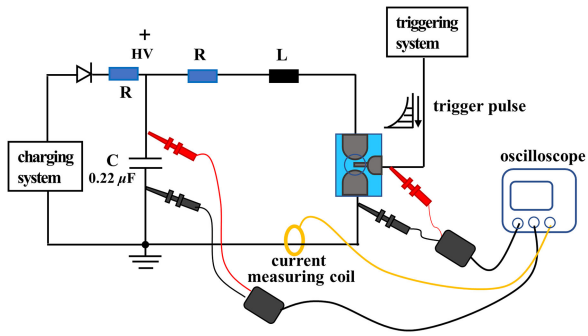

Fig. 3. Equivalent-circuit molded for the characterization of the planar trigger switch.

The exploded view of fabrication process of the planar trigger switch was presented in Fig. 2. Starting from the bottom, the tamper was formed by 1–10 layers of green sheets, and each sheet had a thickness of 110 μm. Metal layer 11 was about 12-μm-thick Au slurry printed on the 10th layer, served as switch electrodes. Above the Au slurry, 15-μm-thick Pd/Ag (gray areas) was coated on the switch electrodes. The Pd/Ag layer was to easily connect with the external circuit components, and to decrease the ablation of the electrodes during the actuation of the switch. Layers 12–20 were also made up of 110-μm-thick green sheet, acting as the structure of the switch groove and pad grooves. All the grooves mentioned above were punched by a mechanical punch. After the processing of each layer was completed, they were stacked and pressed in an orderly way, and combined into a laminated substrate. Then, the laminated substrate was put into a cofiring furnace to make the Au slurry and the green sheets simultaneously sintered at 900 °C.

B. Experimental Device

In order to carry out the corresponding experiments on the planar trigger switch, a simple experimental device was designed, as shown in Fig. 3. This device consisted of a constant current charging system, a high-voltage pulse power capacitor, a planar trigger switch, a triggering system, and a measurement system. The charging voltage of the constant current charging system was adjustable, and the rising rate of the voltage was

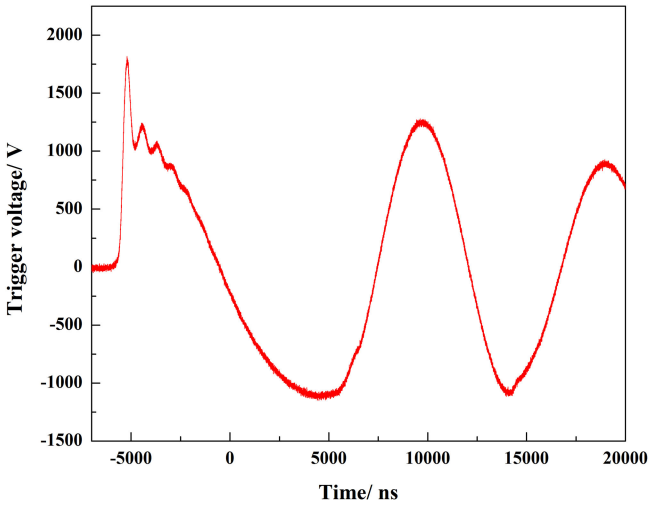

Fig. 4. Typical trigger voltage waveform.

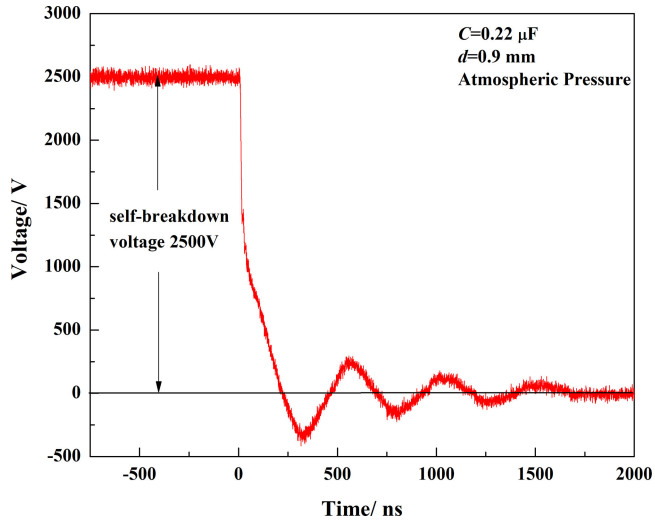

Fig. 5. Typical self-breakdown voltage waveform.

approximately 20 V/s. The trigger system used in this experiment could output a trigger pulse with an adjustable voltage, specifically with 670 ns rise front. The typical trigger pulse waveform was shown in Fig. 4. In this experiment, the trigger pulse amplitude was approximately 1800 V. This high-voltage triggering could keep the trigger electrode at a certain distance from the main gap, and reduce the ablation of the trigger electrode via the high current arc in the main gap of the switch, thus improve the stability and life of the switch. The measuring system included high-voltage differential probes, a Rogowski coil, and a multichannel digital oscilloscope. The high-voltage differential probes were utilized to gauge the trigger signal dropped across the trigger electrode and cathode, as well as the real-time voltage between both sides of the capacitor. The Rogowski coil was used to measure the current through the switch with a sensitivity of 1 V/kA. Finally, both the voltages and current waveform were recorded by the oscilloscope. When the high-voltage capacitor was charged to a certain voltage, a trigger pulse generated by the pulse transformer was coupled to the trigger electrode through a coupling capacitor, causing the switch to turn ON and the high-voltage capacitor to discharge in the circuit. A series of experimental studies on the electrical performance were carried out, including that the static self-breakdown voltages, the delay time, and the jitter under different operating voltages, as well as the inductance and resistance.

C. Self-Breakdown Voltage

The self-breakdown voltage (U_b) was a critical parameter for the spark gap switch. Paschen's law [20] states that if the product of the gas pressure and the gap distance is constant, the self-breakdown voltage of a gas gap is invariant. Usually, the operating voltage range of a gas spark switch was very limited and the self-breakdown voltage was an absolute upper limit. We were interested in measuring U_b of the planar trigger switch with a gap spacing of 900 μm in the atmosphere. For the self-breakdown voltage experiment, two main electrodes were connected to the positive and negative poles of capacitor, respectively, the trigger electrode was suspended, and an increasing voltage was applied across the gas gap and the capacitor. When the voltage between the main electrodes exceeded the self-breakdown voltage of the gap, the capacitor would discharge through the gap immediately. In this experiment, the high-voltage differential probe was placed at both ends of the main electrode and LeCory oscillograph was employed to monitor the voltage drop waveform between the main electrodes. When the gap was broken down, the self-breakdown voltage waveform was obtained. The above procedure was repeated ten times and the mean value of U_b was 2584 V with a standard deviation of 161 V, and the minimum value of U_b was 2400 V. Fig. 5 shows the typical self-breakdown voltage waveform of the planar trigger switch.

D. Delay Time and Jitter

Delay time (τ_d) was another significant parameter used to characterize switch capability. In this paper, we defined τ_d as the time from the abrupt drop of the trigger voltage to the start of the current in the circuit, as shown in Fig. 6. The switch jitter (S) was the standard deviation of the delay time, and it can be used as a sensitivity indicator of switch stabilization. To illustrate the relationship between delay time (τ_d) and the operating voltage, we carried out 80 shots on the planar trigger switch under four different operating voltages, and the voltage was repeatedly from 1500 (about 58% of U_b) to 2250 V (about 87.1% of U_b) in 250 V increments. Adopting the Grubbs criterion, the significance level was set to 0.05 (equivalent to a 95% confidence level), and the abnormal data were eliminated. Fig. 7 shows the average value of τ_d and its error bar (i.e., switch jitter) at four operating voltages. According to Fig. 7, the mean value of τ_d decreased with an increase in the operating voltage because the ionization coefficient α and electron drift velocity v_i were proportional to E/p, where E was the electric field strength and p was the gas pressure [22]. Therefore, at the same pressure and gap distances, the operating voltage was higher, the ionization coefficient α and the electron drift velocity vi were larger, and the delay time τ_d was reduced naturally. In addition, the switch jitter increased

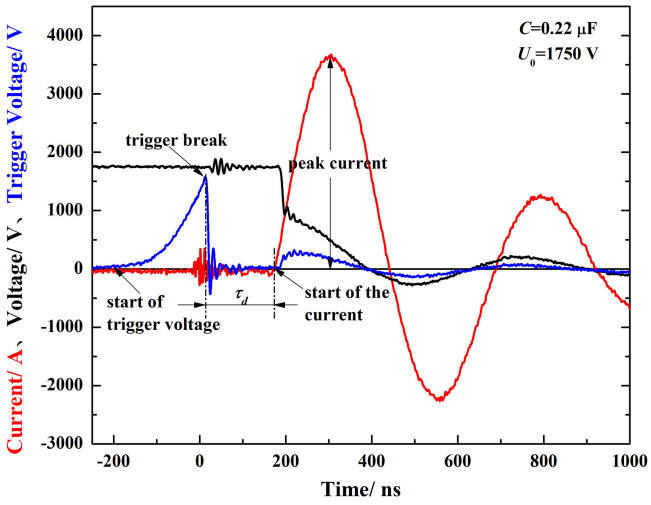

Fig. 6. Typical delay time waveform.

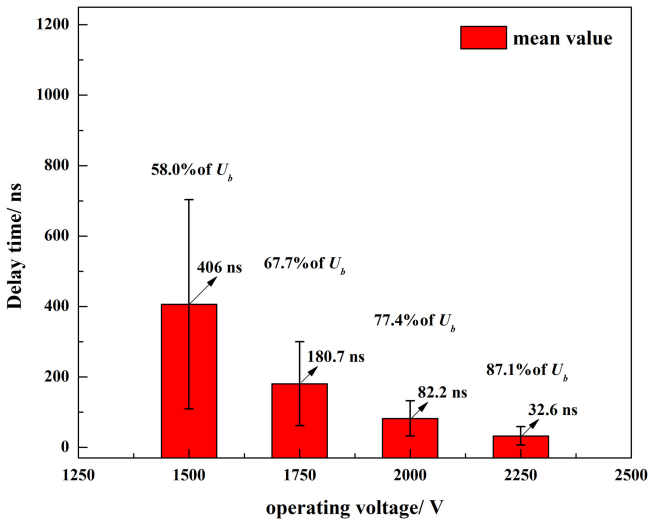

Fig. 7. Mean value of τ_d and switch jitter under four operating voltage.

rapidly as the operating voltage drop below 58% of U_b. When the operating voltage was more than 77.4% of U_b, the switch jitter was not obvious (<50 ns), and the mean value of τ_d was small (no more than 83 ns). Consequently, the switch was more stable when it operated within the range of 77.4%–87.1% of U_b. In practice, gas switches operated no higher than 80% to 90% of U_b. Generally, two considerations determined the maximum operating voltage: 1) allowance for unit-to-unit variations of U_b, and 2) reliability against prefire [13]. Prefire, also called a hold-off failure, meant that the switch was closed without receiving a trigger pulse. When the operating voltage did not exceed 2250 V (87.1% of U_b), no prefire occurred during the charging process. Therefore, we considered that the maximum reliable operating voltage without prefire was 2250 V. Triggering below 58% of U_b was possible, however, the delay time and the jitter were generally very high, and eventually no-fire failures occurred.

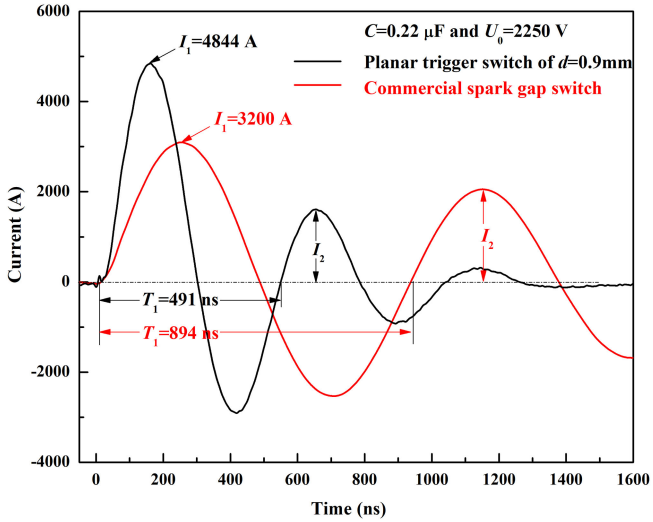

Fig. 8. Current waveforms of two kinds of switches.

E. Inductance Calculation

Resistance and inductance were both major parameters affecting the circuit current magnitude and the switching speed. The discharge circuit shown in Fig. 3 could be treated as a simple *RLC* circuit, which was composed of capacitor, switch, transmission wires, and all the solders point. *C* represented the capacitor and *L* and *R* represented the lumped inductance and resistance, respectively. When the switch was closed, the circuit equation could be described by

$$L\frac{di}{dt}+\frac{1}{C}\int idt+iR=U_0 \tag{3}$$

where U_0 was the initial voltage of the capacitor and L and R were treated as constants. The current could be calculated from (3)

$$i(t)=\frac{U_0}{\omega L}\exp(-\delta t)\times\sin\omega t \tag{4}$$

where

$$\delta=\frac{R}{2L},\ \omega=\sqrt{\frac{1}{LC}-\frac{R^2}{4L^2}}$$

the lumped L and R could be calculated from (4), and the expressions were as follows:

$$R=\frac{2L}{T_1}\ln\frac{I_1}{I_2} \tag{5}$$

$$L=\frac{{T_1}^2}{C}\left[4\pi^2+\left(\ln\frac{I_1}{I_2}\right)^2\right]^{-1} \tag{6}$$

where I_1 and I_2 were the first peak current and the second peak current, respectively, and T_1 was the first discharge period. In the same test device, we measured the discharge parameters of the planar trigger switch and the commercial triggered spark gap switch, respectively. The lumped inductance and resistance of the circuit were calculated from (5) and (6). Fig. 8 shows the current waveforms of the two kinds of switches, and Table I

TABLE I
CALCULATION OF LUMPED INDUCTANCE AND RESISTANCE OF THE CIRCUIT

Switch type	Operating voltage/V	I_1/A	I_2/A	T_1/ns	L/nH	R/mΩ
Planar trigger switch	2250	4844	1609	491.8	27.0	121.1
	2000	4000	1336	490.0	26.8	120.1
	1750	3680	1270	490.4	26.9	116.8
	1500	2990	926	496.8	27.4	129.6
Commercial triggered spark gap switch	2250	3200	2160	894.4	91.7	80.6
	2000	2840	1920	895.4	91.9	80.4
	1750	2480	1640	891.4	91.1	84.5
	1500	2080	1320	895.6	91.9	93.3

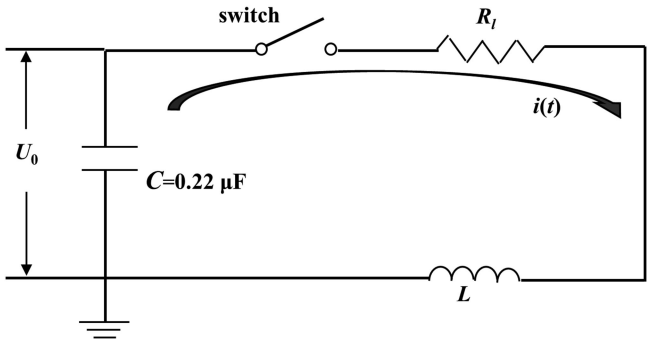

Fig. 9. Circuit model equivariant diagram.

shows the comparisons of the relevant parameters. According to Table I, we found that the lumped inductance of the planar trigger switch was lower than that of commercial switch by approximately 60 nH, the first discharge period T_1 was shortened by nearly 1/2, and the peak current increased by about 30%. Therefore, the use of the planar trigger switch was conductive to reduce the inductance and increase the circuit current, so that the current could be released into the load in a short time.

F. System Modeling

In order to compute the theoretical output waveform of the planar trigger switch, the overall phenomenon of the switch could be modeled by an equivalent circuit consisting of a series combination of inductance and arc resistance and capacitance. Assuming the parasitic capacitance (∼pF) generated by weak ionization discharge could be neglected before a conducting channel was established. The circuit model considered in this paper was a series connection of resistor and inductor. As seen in Fig. 9, the capacitor C in the diagram represented the high-voltage capacitor used in the circuit. The circuit inherent inductance L was considered as a constant that could be calculated by (6). The switch resistance was modeled as a time-varied value R_v, and many empirical formulas to describe the transition from a streamer channel to a low-resistance arc channel have been developed. In this study, we chose the Rompe–Wiezel model [23], [24] because the variable resistance for our testing conditions was similar (1 atm, $d < 0.035$ m). The expression for this model was as follows:

$$R_v(t) = \frac{d}{\sqrt{\frac{2\alpha}{p}\int_0^1 i^2(t)dt}} \tag{7}$$

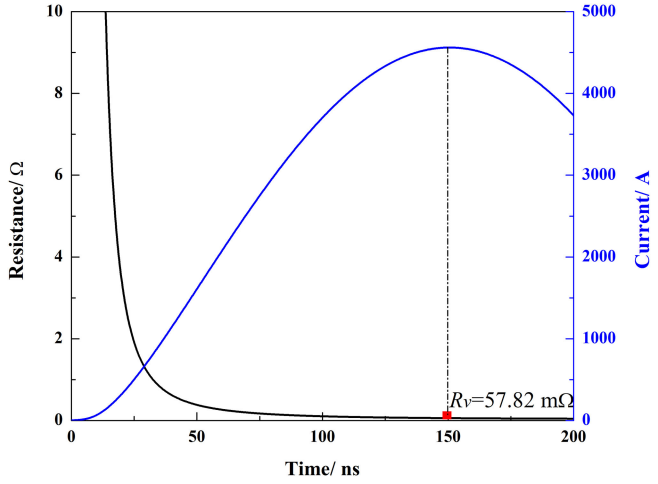

Fig. 10. Theoretical switch spark resistance variation at 0.22 μF/2.0 kV.

where d was the gap distance, p was the gas pressure, $i(t)$ was the current flowing through the switch, and α was a coefficient characterizing the nature of the gas. Its value was 0.08–0.1 MPa·cm^2·s^{-1}·V^{-2} for air and nitrogen. When the switch broke down instantaneously, the circuit equation could be represented as

$$\frac{1}{C}\int i(t)dt + L\frac{di}{dt} + R_v(t)\cdot i(t) + R_l\cdot i(t) = U_0 \tag{8}$$

where R_l was loop resistance, and U_0 was the initial voltage. Assuming the capacitance voltage was $U_C(t)$, then (8) could be divided into the following two formulas (9) and (10):

$$i(t) = -C\frac{dU_C(t)}{dt} \tag{9}$$

$$U_C(t) = L\frac{di}{dt} + [R_v(t) + R_l]\cdot i(t) \tag{10}$$

the differential of (7) was

$$\frac{dR_v(t)}{dt} = -\frac{\alpha}{pd^2}{R_v}^3(t)i^2(t) \tag{11}$$

the constants were as follows: $C = 0.22$ μF, $p = 0.1$ MPa, $\alpha = 0.09$ MPa·cm^2·s^{-1}·V^{-2}, $d = 0.9$ mm, $L = 27$ nH (the average value of 80 times measurement). Since R_l was unknown, we assumed that there was no resistance in the circuit besides the time-varied switch spark resistance R_v, that was, $R_l = 0$ mΩ. The initial conditions were $U_C(t) = 2000$ V, $i(0) = 0$, and $R_v \to \infty$. Then, the switch spark resistance versus the time curve could be obtained by using numerical methods to solve (9)–(11). Fig. 10 shows $R_v - t$ and I-t curves at $R_l = 0$ mΩ. From Fig. 10, it was clear that the switch spark resistance R_v was 57.82 mΩ, corresponded to the first peak current. With formula (5), we calculated the circuit total resistance R to be 111.17 mΩ, which was the average value of 20 measurements. Therefore, the loop resistance $R_l = R - R_v$ could be roughly estimated as 53.35 mΩ. Using the same method, the computed mean value of R_l was 50.87 mΩ under four different initial voltages. Substituting $R_l = 50.87$ mΩ into (10), the output current and voltage waveforms of the planar switch could finally be obtained.

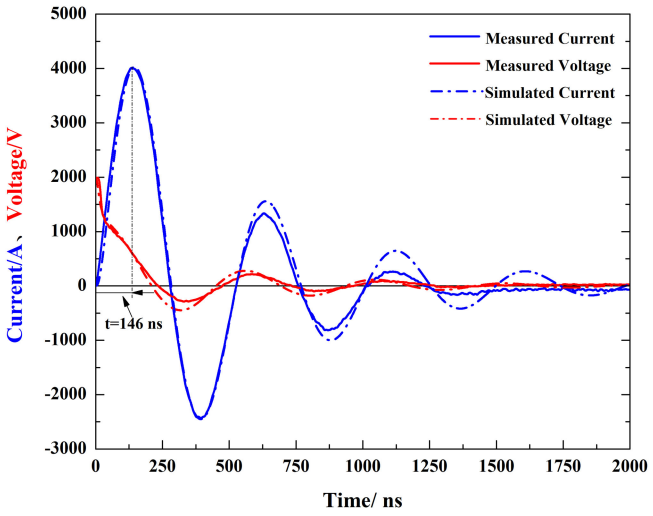

Fig. 11. Contrast of measured and theoretical output waveforms of planar trigger switch at 0.22 μF/2.0 kV.

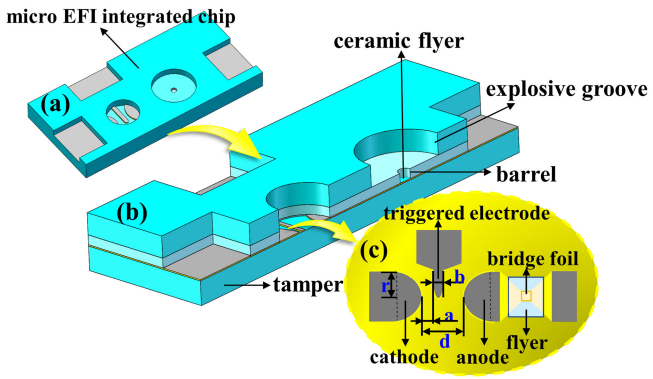

Fig. 12. (a) 3-D illustration of the S-EFI chip inserted with planar trigger switch. (b) Sectional view of chip. (c) Top view of metal layer.

Fig. 11 shows the comparisons of the measured switch current and voltage waveforms with the theoretical ones. As shown in Fig. 11, the simulated results had a good agreement with the experimental results, especially for the first peak current of 4000 A and the rising time of 146 ns. The results indicated that the Rompe–Wiezel model could preferably simulate the performance of the planar trigger switch.

III. Characterization of the S-EFI Chip

A 3-D illustration of the S-EFI chip was shown in Fig. 12(a). This chip was formed by *in situ* inserting EFI in series with the planar trigger switch. Fig. 12(b) shows the sectional view of the chip. As depicted in Fig. 12(c), a 12-μm-thick Au slurry, printed on the tenth layer, preformed as the switch electrodes and the transition zone of the exploding foil changing from wide to narrow. The bridge foil (400 μm $\times$ 400 μm $\times$ 4.5 μm) was the narrowest portion of the metal layer, which was patterned above the transition zone separately. In addition, a 50-μm-thick green sheet was placed on the top of the bridge foil, which played the part of a flyer. In order to reduce the parasitic impedance

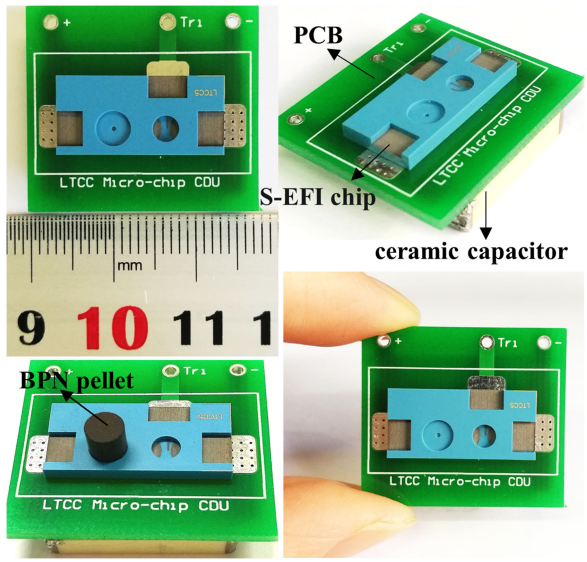

Fig. 13. Miniature firing device consists of a S-EFI chip, a PCB, and a high-voltage ceramic capacitor.

of the transmission line and improve the energy efficiency, we designed a miniature firing device, as shown in Fig. 13. This device consisted of a S-EFI chip, a printed circuit board (PCB), and a high-voltage ceramic capacitor, thereby forming a sandwich structure. In this section, the performance of the S-EFI integrated chip was analyzed below in three related approaches: 1) by considering of the current and voltage waveform in the circuit, 2) by investigating the details of the acceleration process of the ceramic flyer, and 3) by validating the high-velocity flyer impact experiment.

A. Electrical Characteristics

The schematic diagram of the action process of the S-EFI chip was portrayed in Fig. 14. First, the capacitor was charged to a needed voltage. When the high-voltage signal reached the trigger electrode, the voltage across the trigger electrode and the cathode exceeded the breakdown voltage bias of the air gap between them, so the switch was triggered. Electrons and ions in the left area between the trigger electrode and the cathode represented the initial ionization. After the switch was triggered, the plasma generated in the left gap subsequently propagated into the right gap, causing further gas ionization [25]. After that, the conduction of the two main electrodes was achieved, and the capacitor began to discharge from the low-impedance ionized gas, ultimately forming a high pulsed current in the loop. When the high current passed through the narrowest exploding foil, the intense joule thermal deposition enabled the physical state of the metal bridge foil to change dramatically, resulting in the excitation of the shock wave and electromagnetic radiation. Finally, the shock wave compressed the ceramic flyer and drove the flyer to move. The flyer was cut into a small disc under the restraint of the barrel, to impact the explosive at a speed of several km/s, thereby initiating the explosive.

Current density J_B at burst time was an important factor affecting flyer speed v_f. J_B could be defined as the ratio of

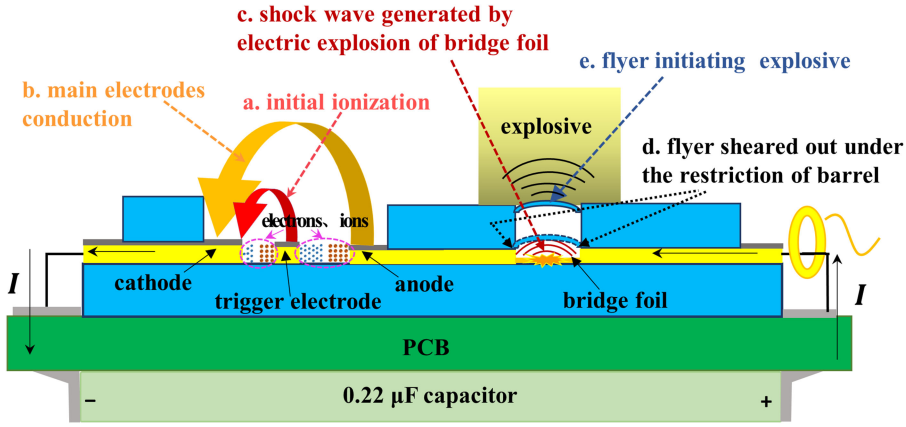

Fig. 14. Schematic diagram of the S-EFI chip for electrical characterization.

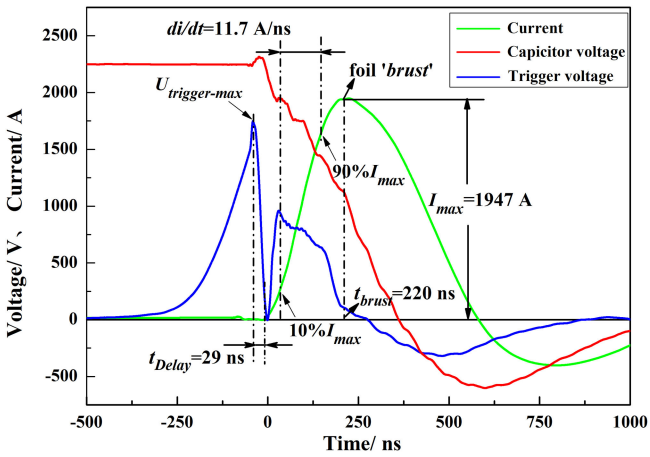

Fig. 15. Typical electrical property for the S-EFI chip.

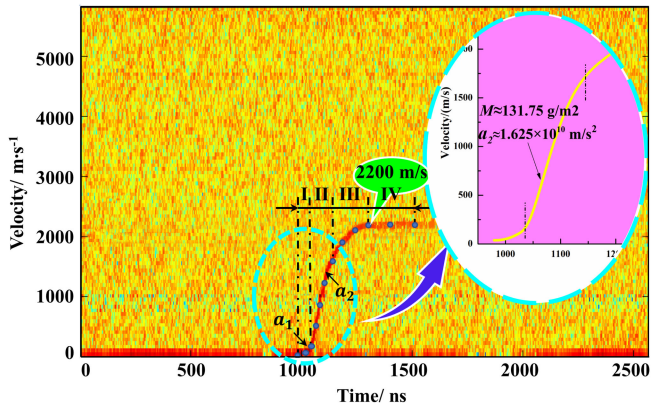

Fig. 16. PDV spectrogram of 50-μm-thick ceramic flyer.

current to cross-sectional area of bridge foil when electroexplosion occurred. According to the Tucker–Stanton model [26], when the parameters of bridge foil and flyer were determined, flyer speed depended only on the burst current density J_B. The relation was as follows:

$$v_f = \sqrt{kJ_B^b}\left(\frac{M}{C}+\frac{1}{3}\right)^{-\frac{1}{2}} \tag{12}$$

where k and b were empirically determined constants, M was the mass per unit area of the flyer, C was the mass per unit area of bridge foil, and v_f was proportional to J_B. Therefore, reducing the circuit inductance and increasing the burst current would be propitious to improve v_f and reduce the ignition energy. Fig. 15 shows the typical electrical characteristics at 0.22 μF/2.25 kV. The switch delay time was only 29 ns, and the peak current was 1947 A. The current was delivered into the exploding foil at a rising rate of 11.7 A·ns^{-1}. The current density J_B was calculated as 1.08×10^8 A·cm^{-2}, implying that a fast-electrical explosion phenomenon ($J \geq 10^8$ A·cm^{-2}) was aroused in the foil [27]. In most studies, the burst time ($t_{\rm burst}$) for an EFI could be defined as the spike point on the voltage waveform where the current began to reverse direction [28]. In this test, $t_{\rm burst}$, which was determined by the criterion $dI/dt = 0$, was consistent with a peak current time of 220 ns.

B. Real-Time Velocity Measurement of Ceramic Flyer

The flyer velocity was commonly used as a vital metric to describe the initiation ability of an EFI. Photon Doppler velocimetry (PDV) could provide high accuracy monitoring of the velocity history for a moving object. The fundamental principle of PDV was the coherent interference between the initial light and the light reflected from the moving subject, thereby forming a frequency difference signal with changes in light intensity. In our home-built PDV measurement system, the interference frequency of 1.29 GHz corresponded to a movement speed of 1 km/s. A semiconductor photodetector was applied to convert the optical signals to electrical signals, which was later recorded by a four-input high-speed digital oscilloscope with a bandwidth of 33 GHz at a sampling rate of 80 GS/s. Fig. 16 displays the PDV spectrogram of the ceramic flyer with a terminal speed of 2200 m/s at 2.25 kV, and each phase of this acceleration process could be observed.

According to Fig. 16, the flight course of the ceramic flyer could be divided into four stages. In the first stage, the bridge foil had not burst yet, and the flyer remained nearly at rest.

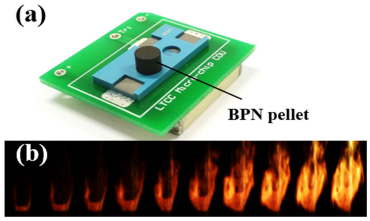

Fig. 17. (a) Picture of firing device with BPN pellet. (b) High-speed photography of BPN combustion.

However, the magnetic pressure P_B exerted by the current tended to drive the flyer at a fairly slow speed. After the metal bridge foil burst, the flyer was accelerated by both the foil expanded plasma thermal pressure P_T and the magnetic pressure P_B [29], with an approximate acceleration of 1.625×10^{10} m/s^2 in the second stage. Subsequently, with the constant expansion of the metal products, the slope of the flyer velocity was depressed in the third phase due to the sharp reduction of the density of metal vapor or plasma. At the last stage, the flyer achieved a steady flight due to the balance of the accelerating pressure and the air-resistance. A magnetic field was generated when a high pulsed current passed through the foil. Since the magnetic field $B = \mu_0 I/w$ was determined by the width of bridge foil w (m) and the current flowing through the bridge foil I (A), P_B, which was the equivalent pressure of the magnetic force $J \times B$, could be easily calculated by $\mu_0 J^2/2$ ($J = I/w$). The net pressure P_F on the flyer could also be roughly deduced from Newton's law $P_F = Ma$, where M was the mass per unit area of flyer and a was the acceleration obtained from the speed–time curves. Therefore, the maximum values of P_B and P_F were calculated to be 14.88 MPa and 2.14 GPa, respectively. From these results, one can also conclude that the metal thermal expansion pressure P_T was the main contributor to the flyer movement.

C. Firing Test

The main factor of initiating explosive depended on the impact pressure of flyer. In order to perform the high-velocity flyer impact targets experiments, the ignition and initiation tests were implemented on the firing device. Standard Boron–potassium nitrate (BPN) powder and hexanitrostilbene (HNS) powder were pressed into pellets with a height and diameter of 4 mm. Fig. 17(a) shows a photograph of a BPN pellet placed in the explosive groove, and Fig. 17(b) shows the combustion process of the BPN captured by high-speed photography. The tests indicated that 1.3 and 2.4 kV were the minimum ignition and detonation voltages of the BPN and HNS explosives, respectively. The detonation threshold of impact pressure varied with the type of explosives, and the impact initiation pressure of HNS was much higher than that of BPN. According to the equation of shock wave [30], the higher the flyer velocity, the greater the pressure formed by flyer impact. When the operating voltage was larger, the higher the circuit current, then the higher velocity of the flyer obtained, thus the greater the impact pressure.

IV. Conclusion

In this paper, a cost-effective planar trigger switch that can be manufactured in batch by LTCC has been demonstrated. The test results show that the peak current and the rise time are about 4000 A and 146 ns at 0.22 μF/2.0 kV, respectively, when the main electrodes gap distance was 0.9 mm. It was generally in agreement with the simulated ones. Compared with the commercial spark gap switch, this switch has the advantages of lower inductance, larger current, and easier to connect with strip transmission lines, which is alternative to the more expensive commercial ones and promising in pulsed power applications. On this basis, the planar trigger switch was designed specifically to be *in situ* integrated with an EFI for initiation systems. This compact construction can significantly reduce the volume of initiation systems and the parasitic inductances, thus enhance the driving capacity of EFI.

References

[1] D. V. Keller and J. R. Penning, "Exploding foils—The production of plane shock waves and the acceleration of thin flyer plates," in *Exploding Wires*. Boston, MA, USA: Springer, 1962, pp. 263–277.

[2] A. H. Guenther, D. C. Wunsch, and T. D. Soapes, "Acceleration of thin plates by exploding foil techniques," in *Exploding Wires*. Boston, MA, USA: Springer, 1962, pp. 279–298.

[3] J. E. Osher, R. Gathers, H. H. Chau, R. S. Lee, G. Pomykal, and R. C. Weingart, "Hypervelocity acceleration and impact experiments with the LLNL electric gun," *Int. J. Impact Eng.*, vol. 10, no. 1–4, pp. 439–452, 1990.

[4] H. R. Davies, D. J. Chapman, T. A. Vine, and W. G. Proud, "Characterization of an exploding foil initiator (EFI) system," *AIP Conf. Proc.*, vol. 1195, pp. 283–286, 2009.

[5] T. M. Willey *et al.*, "X-ray imaging and 3D reconstruction of in-flight exploding foil initiator flyers," *J. Appl. Phys.*, vol. 119, no. 23, Jun. 2016, Art. no. 235901.

[6] M. Bowden and W. Neal, "High fidelity studies of exploding foil initiator bridges, Part 1: Experimental method," *AIP Conf. Proc.*, vol. 1793, 2015, Art. no. 060020.

[7] Z. F. Song, J. J. Mo, J. H. Zhao, F. L. Tan, and H. Yuan, "Study on launching technique of a 98kJ electric gun for hypervelocity impact experiments," *Int. J. Impact Eng.*, vol. 122, pp. 419–430, Dec. 2018.

[8] F. T. Warren, J. M. Wilson, J. E. Thompson, R. L. Boxman, and T. S. Sudarshan, "Vacuum switch trigger delay characteristics," *IEEE Trans. Plasma Sci.*, vol. PS-10, no. 4, pp. 298–301, Dec. 1982.

[9] N. Idir, R. Bausiere, and J. J. Franchaud, "Active gate voltage control of turn-on di/dt and turn-off dv/dt in insulated gate transistors," *IEEE Trans. Power Electron.*, vol. 21, no. 4, pp. 849–855, Jul. 2006.

[10] K. Fujii, P. Koellensperger, and R. W. D. Doncker, "Characterization and comparison of high blocking voltage IGBTs and IEGTs under hard- and soft-switching conditions," *IEEE Trans. Power Electron.*, vol. 23, no. 1, pp. 172–179, Jan. 2008.

[11] H. Wang, A. Q. Huang, and F. Wang, "Development of a scalable power semiconductor switch (SPSS)," *IEEE Trans. Power Electron.*, vol. 22, no. 2, pp. 364–373, Mar. 2007.

[12] T. R. Mcnutt, A. R. Hefner, H. A. Mantooth, D. Berning, and S. H. Ryu, "Silicon carbide power MOSFET model and parameter extraction sequence," *IEEE Trans. Power Electron.*, vol. 22, no. 2, pp. 353–363, Mar. 2007.

[13] K. W. Chu and G. L. Scott, "A comparison of high-voltage switches," Office of Scientific and Technical Information Technical Reports, Sandia National Labs., Albuquerque, NM, USA, Tech. Rep. SAND99-0154, 1999.

[14] Z. W. Zhou, G. P. Ding, Z. Q. Yang, W. J. Lu, and S. Hui, "A micromachined pulsed power switch based on Kapton films," in *Proc. IEEE Int. Conf. Adv. Technol. Design Manuf.*, Beijing, China, 2010, pp. 439–442.

[15] C. Xu, P. Zhu, K. Chen, W. Zhang, R. Shen, and Y. Ye, "A highly integrated conjoined single shot switch and exploding foil initiator chip based on MEMS technology," *IEEE Electron Device Lett.*, vol. 38, no. 11, pp. 1610–1613, Nov. 2017.

[16] T. A. Baginski and K. A. Thomas, "A robust one-shot switch for high-power pulse applications," *IEEE Trans. Power Electron.*, vol. 24, no. 1, pp. 253–259, Jan. 2009.
[17] T. A. Baginski, R. N. Dean, and E. J. Wild, "Micromachined planar triggered spark gap switch," *IEEE Trans. Compon. Packag. Manuf. Technol.*, vol. 1, no. 9, pp. 1480–1485, Sep. 2011.
[18] Y. Imanaka, *Multilayered Low Temperature Cofired Ceramics (LTCC) Technology*. New York, NY, USA: Springer, 2005, pp. 1–16.
[19] L. J. Golonka, "Technology and applications of low temperature co-fired ceramic (LTCC) based sensors and microsystems," *Bull. Polish Acad. Sci. Tech. Sci.*, vol. 54, no. 2, pp. 221–231, Jun. 2006.
[20] H. Bluhm, *Pulsed Power Systems: Principles and Applications*. Berlin, Germany: Springer-Verlag, 2006, pp. 6–14.
[21] F. Jiang, "Development of electric pulse triggered gas spark switch," M.S. Thesis, Nanjing Agricultural Univ., Jiangsu, China, 2009.
[22] A. J. Davies, C. J. Evans, P. Townsend, and P. M. Woodison, "Computation of axial and radial development of discharges between plane parallel electrodes," *Proc. Inst. Elect. Eng.*, vol. 124, no. 2, pp. 179–182, Feb. 1977.
[23] V. R. Rompe and W. Weizel, "Ueber das Toeplersche Funkengesetz," *Eur. Phys. J. A*, vol. 122, no. 9–12, pp. 636–637, Sep. 1944.
[24] T. G. Engel, A. L. Donaldson, and M. Kristiansen, "The pulsed discharge arc resistance and its functional behavior," *IEEE Trans. Plasma Sci.*, vol. 17, no. 2, pp. 323–329, Apr. 1989.
[25] C. Liu *et al.*, "Design, simulation, and characterization of a low-cost in-plane spark gap microswitch with dual-trigger electrode for pulsed power applications," *IEEE Trans. Ind. Electron.*, vol. 60, no. 8, pp. 3240–3247, Aug. 2013.
[26] T. J. Tucker and P. L. Stanton, "Electrical gurney energy: A new concept of modelling energy transference from electrically exploded conductors," *Sandia Nat. Laboratory Rep.*, Albuquerque, NM, USA, Tech. Rep. 75-0244, 1975.
[27] S. A. Chaikovsky, V. I. Oreshkin, G. A. Mesyats, N. A. Ratakhin, I. M. Datsko, and B. A. Kablambaev, "Electrical explosion of metals in fast-rising megagauss magnetic fields," *Phys. Plasmas*, vol. 16, no. 4, Apr. 2009, Art. no. 042701.
[28] S. E. Goh, "An exploding foil shockwave technique for magnetic flux compression and high-voltage pulse generation," Ph.D. dissertation, Dept. Electron. Elect. Eng., Loughborough Uni., Loughborough, U.K., 2002.
[29] J. E. Osher, G. Barnes, H. H. Chau, and R. S. Lee, "Operating characteristics and modeling of the LLNL 100-kV electric gun," *IEEE Trans. Plasma Sci.*, vol. 17, no. 3, pp. 392–402, Jun. 1989.
[30] S. Ebenhöch, S. Nau, and I. Häring, "Validated model-based simulation tool for design optimization of exploding foil initiators," *J. Defense Model. Simul.*, vol. 12, no. 2, pp. 189–207, 2014.

Qiu Zhang was born in 1993. She received the B.S. degree from the School of Chemical Engineering and Environment, North University of China, Taiyuan, China, in 2016. She is currently working toward the Ph.D. degree at Nanjing University of Science and Technology, Nanjing, China.

Her current research interests include design, simulation, and fabrication of the electroexplosive devices, shock loading, MEMS ignition, and detonation system.

Cong Xu was born in 1993. He received the bachelor's degree from Nanjing University of Science and Technology, Nanjing, China, in 2015, where he is currently working toward the Ph.D. degree at the School of Chemical Engineering.

His research interests include electro-explosion of metal, MEMS, and dynamic loading.

Peng Zhu was born in May 1978. He received the M.S. and Ph.D. degrees from Nanjing University of Science and Technology, Nanjing, China, in 2007 and 2014, respectively.

He was a Visiting Scholar in Homyel State University, Belarus, from 2010 to 2011. He is currently an Associate Professor with the School of Chemical Engineering, Nanjing University of Science and Technology. His research interests include PyroMEMS devices, microreactors, and microfluidics.

Guili Yang was born in October 1981. She received the Ph.D. degree from Beijing Institute of Technology, Beijing, China, in 2010.

She was a Postdoctoral with Nanjing University of Science and Technology from 2010 to 2012. She was a Lecturer at the School of Field Engineering, Army Engineer University of PLA, Chongqing, China, since 2013. Her research activities include MEMS ignition and initiation technology.

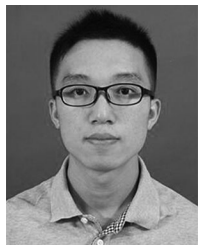

Zhi Yang was born in 1994. He received the B.S. degree from the School of Chemical Engineering, Nanjing University of Science and Technology, Nanjing, China, in 2016, where he is currently working toward the Ph.D. degree.

His research interests include high-speed impact and MEMS devices.

Ruiqi Shen was born in June 1963. He received the M.S. and Ph.D. degrees from Nanjing University of Science and Technology, Nanjing, China, in 1986 and 1991, respectively.

He was a Visiting Scholar with Mendeleyev University of Chemical Technology, Russia, from 2001 to 2002. He was a Professor with the School of Chemical Engineering, Nanjing University of Science and Technology, since 2000. His research interests include MEMS devices, microfluidics, nanoenergetic materials, laser physics, and chemistry.